A new homologous series of semi-conducting liquid crystals based on phenyl-anthracene: synthesis and effect of the alkyloxy terminal chain on charge transport and photoconductive properties

A. Moghnieh, Pierre-Edouard Danjou, Yahia Boussoualem, K. Ferchichi, Abdelylah Daoudi

A new homologous series of semi-conducting liquid crystals based on phenyl-anthracene: synthesis and effect of alkyloxy terminal chain on charge transport and photoconductive properties

A. MOGHNIEH,*[a] P.-E. DANJOU,[b] Y. BOUSSOUALEM,[a] K. FERCHICHI,[a] and A. DAOUDI[a]

[a] *Univ. Littoral Côte d'Opale, UR 4476 - UDSMM - Unité de Dynamique et Structure de Matériaux Moléculaires, 59140 Dunkerque, France.* * *E-mail: abir.moghnieh@univ-littoral.fr* [b] *Univ. Littoral Côte d'Opale, UR 4492-UCEIV-Unité de Chimie Environnementale et Interactions sur le Vivant, 59140 Dunkerque, France.*

The π-conjugate system is the key to charge transport properties in organic semiconductors. Four multifunctional mesogenic materials were designed and synthesised from 2-amino anthracene and para-hydroxybenzaldehyde. Each material contains a central, rigid phenyl-anthracene core and one flexible alkyloxy chain with different lengths based on the concept of combining liquid crystal (LC) materials featuring facile processability, highly ordered alignment, and effective charge transport. (E)-N-(anthracen-2-yl)-1-(4-(alkyloxy) phenyl) methanimine (n-OPIA) with n = 8, 10, 12, and 16 was chemically characterized by nuclear magnetic resonance spectroscopy and high-resolution mass spectrometry. Their thermal behaviours were performed by means of differential scanning calorimetry, and polarised optical microscopy and showed differences in mesomorphic behaviours with respect to the alkyloxy chain length. Concerning their frontier molecular energy levels, they were studied by optical spectroscopy and cyclic voltammetry and compared to values obtained via ab initio density-functional theory (DFT) calculations. The LC Field-Effect Transistors (LC-FETs) using solvent vapour enhanced drop casting based n-OPIA material showed efficient electrical parameters and interesting photoconductive properties, indicating their potential applications in multifunctional integrated devices. As the alkyloxy chain length of the n-OPIA compounds increased, the hole mobility, on/off current ratio, and responsivity decreased. The 8-OPIA homologous exhibits a mobility one order of magnitude larger than the previously studied homologue namely 10-OPIA.

1 Introduction

Over the past two decades, organic semiconductor materials have attracted the attention of researchers in numerous applications such as light-emitting diodes (OLEDs), photovoltaic cells (OPVs) and field-effect transistors (OFETs),[1,2] compared with inorganic materials, which are characterized by difficult modifications to molecular structures, complex and costly manufacturing approaches, and a lack of flexibility.[3,4] The semiconducting characteristics in organic materials originate from the π-conjugated systems as polymers, oligomers as well as small molecules.

Among the π-conjugated small molecules the anthracene is one that shows intermolecular overlap resulting from a strong and persistent π-π* coupling that provides excellent performances in organic electronics.[5,6] The anthracene offers a vast array of positions to add groups in end (2, 3, 6, 7) and peri (1, 4, 5, 8, 9, 10) positions. Several aromatic groups were added in the end positions (thiophene,[7] naphthalene,[8] phenyl,[9] anthracene[10]) to increase the π-conjugation system and later on the charge mobility since the last few decades,[11] and other groups like alkyl and alkyloxy chains to enhance the solubility and simplify the processability of these materials. For example, the (triisopropylsilyl)ethynyl TIPS functional group is an excellent group that enhances the solubility of anthracene derivatives in organic solvents. This is demonstrated by the addition of a naphthalene substitution in the 2,6 positions of the 9,10-TIPS-functionalised molecule, which achieved a hole mobility of μ = 3.7 cm²/V s.[12]

To further enhance semiconductor performance, the integration of liquid crystal properties has been investigated. Liquid crystals offer a promising solution to improve the molecular orientation of semiconductors in the film, thereby enhancing their mobility.[13–16] These materials, comprising π-conjugated cores and non-carrying molecular fragments such as alkyl and alkyloxy chains, induce phase segregation between flexible insulating parts and rigid conducting parts.[17] Overall, liquid crystals with well-aligned orientation and acceptable processability are considered promising candidates to serve as active materials in high-performance optoelectronic devices for future flexible organic electronics.

The purpose of this work is to expand on and complete our previous research, which focused on the synthesis and characterization of a novel semiconductor with mesogenic features, namely 10-OPIA,[18] a member of our newly synthesized homologous series. This series

of semiconductors is constituted of two important parts: a π-conjugated core (anthracene-phenyl) that allows charge transport, and non-carrying molecular fragments in the form of an alkyloxy chain that contribute to structural flexibility and mesomorphic behaviour. We have extended our investigation here to examine the impact of varying the alkyloxy chain length of the homologous series, (E)-N-(anthracen-2-yl)-1-(4-(alkyloxy) phenyl) methanimine (n-OPIA) on their mesomorphic behaviour as well as on the electrical parameters and photoconductive properties relevant to the applications in organic field-effect transistors (OFETs) and photo-effect transistors (OPETs).

Initially, the synthesis process entails two distinct stages, encompassing alkylation and imine coupling, leveraging commercially available starting materials. Subsequent validation of the synthesised compounds involves meticulous analysis utilizing advanced techniques such as nuclear magnetic resonance (NMR) and mass spectroscopy to ensure the desired chemical structures are achieved. Moving forward, a comprehensive characterization of energy levels is conducted through cyclic voltammetry and optical spectroscopy (UV-vis), allowing for a thorough comparison with expected molecular orbital levels derived from ab initio calculations. Furthermore, mesomorphic measurements are undertaken utilizing differential scanning calorimetry (DSC) and polarized optical microscopy (POM), shedding light on the structural arrangements within the materials and their response to changes in temperature and alignment. Lastly, the practical utility and multifunctional potential of the synthesised compounds are put into active layers to test their performance on OFET devices. These evaluations are performed under both ambient and controlled conditions, including in darkness and under UV illumination at 455 nm, providing crucial insights into the materials' performance across various operating scenarios showing that the hole mobility, on/off current ratio, and responsivity of the n-OPIA compounds decrease with increasing alkyloxy chain length. The measured mobility of 8-OPIA is one order of magnitude larger than that for our previously described homologues, the 10-OPIA. Through this comprehensive approach, the homologous series aims to not only advance fundamental understanding but also pave the way for the development of tailored materials for future optoelectronic applications.[19]

2 Experimental details

2.1 Materials.

2-aminoanthracene (Alfa Aesar, 94 %), 1-Bromobutane (Acros, 99 %), 1-Bromooctane (Aldrich, 99 %), 1-Bromodecane (Alfa Aesar, 98 %), 1-Bromododecane (Acros, 98 %), 1-bromohexadecane (Acros, 97 %), 4-hydroxy-benzaldehyde (Aldrich, 98 %), glacial acetic acid, and potassium carbonate were used as received. Chloroform-d was dried over K_2CO_3 before use. The solvents were used without purification.

2.2 Techniques.

^{1}H NMR spectral data were obtained on a Bruker Avance III 400 MHz spectrometer. Mass spectra were performed on an Agilent 6540 UHD Q-TOF LC/MS system. DSC was performed on TA Instruments Q1000 1 with a heating and cooling rate of 10 °C /min. DFT calculations were carried out by Gaussian 09, B3LYP functional, and 6-31++G(d,p) basis set. UV-vis absorption spectra were recorded on a PerkinElmer Lambda 2 spectrometer. For liquid state measurements, the solution was prepared in dichloromethane (10^{-5} M) and placed in a standard quartz cuvette with an optical path length of 1 cm. For solid-state measurements, the films were drop-casted onto quartz substrates from a chlorobenzene solution (4 mg/mL). The analysis was taken over a range of wavelengths from 230 nm to 500 nm. Cyclic voltammetry was carried out on a Metrohm AUTOLAB PGSTAT302. The solution was prepared from n-OPIA (2 mmol/L) in dichloromethane and tetrabutylammonium hexafluorophosphate $TBAPF_6$ (0.1 M) as a supportive electrolyte, mixed (2h), and put in the electrochemical cell. The electrochemical cell was deoxygenated with argon for 20 minutes before measurement. Cyclic voltammograms were collected over the voltage range of -2.2 V to 1.8 V, employing a silver wire as a pseudo-reference electrode (RE), a platinum disc of 3 mm diameter as a working electrode (WE), and a platinum wire as a counter electrode (CE). The scan rates varied from 50 to 500 mV/s. 2 ml of a 1 mmol solution of ferrocene (Aldrich, 98%) in supporting electrolyte was added to the cell after collecting the n-OPIA voltammograms and deoxygenated with argon for 20 minutes prior to measurement. Further data were collected to include the potential range of the Fc/Fc^+ oxidation process to extract its half-wave potential (mean value between the anodic and cathodic peaks) and act as a reference for previous n-OPIA data. The film thicknesses were measured using a Deltak XT profilometer. Electrical measurements were carried out using two Keysight B2901 Source Measure Units (SMUs). POM observations were conducted using an Olympus BX60F5 microscope, while temperature control was achieved using a Linkam LTS 350 hot stage. The cells utilized for texture observation were provided by Instec (Instec Inc., USA) and featured a 25 mm^2 active area and a thickness of 10 µm, with a planar orientation of the sample cells. These cells were filled with the studied compounds in the isotropic phase through the action of capillary forces.

2.3 Synthesis of n-OPIA series.

2.3.1 Alkylated para-hydroxybenzaldehyde Ph-OR.

1 mmol of para-hydroxybenzadehyde (PHB) and 1.2 mmol of n-bromoalkane were dissolved in acetone (6 mL per 1 mmol). 20 mmol of potassium carbonate (K_2CO_3) were added and left under reflux (T = 60 °C) for 2 days. Later, the resulting suspension was filtered to remove K_2CO_3. The solvent was evaporated by rotavapor, and flash chromatography with a mixture of dichloromethane and hexane (1:1) was used to purify the crude product. To finally obtain the n-(alkyloxy) benzaldehyde Ph-OR. The following products have been uniformly prepared:

4-(octyloxy) benzaldehyde Ph-OC_8H_{17} was obtained as white powder (m = 718 mg) in a 75 % yield from 500 mg of PHB. ^{1}H NMR (400 MHz, $CDCl_3$): δ 9.87 (s, 1H, COH) 7.83-7.81 (d, J = 8 Hz, 2H, H-benzene), 6.99-6.97 (d, J = 8 Hz, 2H, H-benzene), 4.03 (t, J = 8 Hz, 2H, OCH_2), 1.84-1.77 (quint, J = 8 Hz, 2H, OCH_2CH_2), 1.49-1.42 (m, 2H), 1.28 (m, 8H), 0.88 (t, J = 4 Hz, 3H, CH_2CH_3).

4-(decyloxy) benzaldehyde Ph-$OC_{10}H_{21}$ was obtained as a white powder (m= 857 mg) in an 80 % yield from 500 mg of PHB. ^{1}H NMR (400 MHz, $CDCl_3$): δ 9.85 (s, 1H, COH) 7.82-7.80 (d, J = 8 Hz, 2H, H-benzene), 6.98-6.96 (d, J = 8 Hz, 2H, H-benzene), 4.03 (t, J = 8 Hz, 2H, OCH_2), 1.83-1.76 (quint, J = 8 Hz, 2H, OCH_2CH_2), 1.48-1.41 (m, 2H), 1.26 (m, 12H), 0.88 (t, J = 4 Hz,3H, CH_2CH_3).

4-(dodecyloxy) benzaldehyde Ph-$OC_{12}H_{25}$ was obtained as a colorless viscous liquid (m=975 mg) in an 82 % yield from 500 mg of PHB. ^{1}H NMR (400 MHz, $CDCl_3$): δ 9.87 (s, 1H, COH) 7.83-7.81 (d, J = 8 Hz, 2H, H-benzene), 6.99-6.97 (d, J = 8 Hz, 2H, H-benzene), 4.03 (t, J = 8 Hz, 2H, OCH_2), 1.84-1.74 (quint, J = 8 Hz, 2H, OCH_2CH_2), 1.49-1.42 (m, 2H), 1.26 (m, 16H), 0.88 (t, J = 4 Hz, 3H, CH_2CH_2).

4-(hexadecyloxy) benzaldehyde Ph-$OC_{16}H_{33}$ was obtained as a colorless viscous liquid (m=1105 mg) in a 78 % yield from 500 mg of PHB. ^{1}H NMR (400 MHz, $CDCl_3$): δ 9.85 (s, 1H, COH) 7.82-7.80 (d, J = 8 Hz, 2H, H-benzene), 6.98-6.96 (d, J = 8 Hz, 2H, H-benzene), 4.03 (t, J = 8 Hz, 2H, OCH_2), 1.83-1.76 (quint, J = 8 Hz, 2H, OCH_2CH_2), 1.48-1.41 (m, 2H), 1.26 (m, 24H), 0.88 (t, J = 4 Hz, 3H, CH_2CH_3).

2.3.2 Imine coupling.

1 mmol of 2-aminoanthracene and 1 mmol of 4-(alkyloxy) benzaldehyde was dissolved in toluene (8.5 mL per 1 mmol). 70 µL of glacial acetic acid (CH_3COOH) were added and left under reflux (T = 110 °C) for 2 days. Upon cooling, the crude product was precipitated and washed in toluene and then acetone. The final product (E)-N-(anthracen-2-yl)-1-(4-(alkyloxy) phenyl) methanimine (n-OPIA) was recrystallized in 3 mL of chloroform. The following products have been uniformly prepared:

(E)-N-(anthracen-2-yl)-1-(4-(octyloxy) phenyl) methanimine (8-OPIA) was obtained as yellow powder (m = 220 mg) in a 42 % yield from 247 mg of 2-aminoanthracene. ^{1}H NMR (400 MHz, $CDCl_3$ passed on K_2CO_3): δ 8.58 (s, 1H, NCH), 8.41 (s, 1H, H anthracene), 8.41 (s, 1H, H-anthracene), 8.04-7.98 (m, 3H, H-anthracene), 7.93-7.92 (d, J = 4 Hz, 2H, H-benzene), 7.72 (s, 1H, H-anthracene), 7.50-7.43 (m, 3H, H-anthracene), 7.02-7.00 (d, J = 8 Hz, 2H, H-benzene), 4.04 (t, 2H, J = 8Hz, OCH_2), 1.86-1.79 (quint, 2H, J = 8Hz, OCH_2CH_2), 1.52-1.45 (m, 2H), 1.39-1.31 (m, 8H), 0.90 (t, J = 8Hz, 3H, CH_2CH_3). HRMS (Q-TOF) calculated for $C_{29}H_{32}NO^+$ ($M+H^+$) m/z 410,2478 found m/z 410,2474.

(E)-N-(anthracen-2-yl)-1-(4-(decyloxy) phenyl) Methanimine (10-OPIA) was obtained as a yellow powder (m = 303 mg) in a 60 % yield from 222 mg of 2-aminoanthracene.^{1}H NMR (400 MHz, $CDCl_3$ passed on K_2CO_3): δ 8.58 (s, 1H, NCH), 8.41 (s, 1H, H anthracene), 8.41 (s, 1H, H-anthracene), 8.03-7.99 (m, 3H, H-anthracene), 7.92-7.90 (d, J = 8 Hz, 2H, H benzene), 7.70 (s, 1H, H-anthracene), 7.48-7.44 (m, 3H, H-anthracene), 7.02–7.00 (d, J = 8 Hz, 2H, H-benzene), 4.05 (t, 2H, J = 8 Hz, OCH_2), 1.86-1.79 (quint, 2H, J = 8 Hz, OCH_2CH_2), 1.51-1.45 (m, 2H), 1.39-1.25 (m, 12H), 0.90 (t, J = 8 Hz, 3H, CH_2CH_3). HRMS (Q-TOF) calculated for $C_{31}H_{36}NO^+$ ($M+H^+$) m/z 438.2791 found m/z 438.2790.

(E)-N-(anthracen-2-yl)-1-(4-(dodecyloxy) phenyl) Methan-imine (12-OPIA) was obtained as a yellow powder (m= 260 mg) in 54 % yield from 200 mg of 2-aminoanthracene. ^{1}H NMR (400 MHz, $CDCl_3$ passed on K_2CO_3): δ 8.58 (s, 1H, NCH), 8.41 (s, 1H, H-anthracene), 8.41 (s, 1H, H-anthracene), 8.04-7.98 (m, 3H, H-anthracene), 7.93-7.92 (d, J = 4 Hz, 2H, H-benzene), 7.72 (s, 1H, H-anthracene), 7.50-7.43 (m, 3H, H-anthracene), 7.02-7.00 (d, J = 8 Hz, 2H, H-benzene), 4.04 (t, 2H, J = 8 Hz, OCH_2), 1.86-1.79 (quint, 2H, J = 8 Hz, OCH_2CH_2), 1.52-1.45 (m, 2H), 1.37-1.28 (m, 16H), 0.89 (t, J = 8 Hz, 3H, CH_2CH_3). HRMS (Q-TOF) calculated for $C_{33}H_{40}NO^+$ ($M+H^+$) m/z 466,3104 found m/z 466,3088.

(E)-N-(anthracen-2-yl)-1-(4-(hexadecyloxy)phenyl) Methan-imine (16-OPIA) was obtained as a yellow powder (550 mg) in a 71 % yield from 167 mg of 2-aminoanthracene. ^{1}H NMR (400 MHz, $CDCl_3$ passed on K_2CO_3): δ 8.58 (s, 1H, NCH), 8.41 (s, 1H, H-anthracene), 8.41 (s, 1H, H-anthracene), 8.04-7.98 (m, 3H, H-anthracene), 7.92-7.90 (d, J = 8 Hz, 2H, H - benzene), 7.70 (s, 1H, H-anthracene), 7.49-7.44 (m, 3H, H-anthracene), 7.02-7.00 (d, J = 8 Hz, 2H, H-benzene), 4.05 (t, 2H, J = 8 Hz, OCH_2), 1.86-1.79 (quint, 2H, J = 8 Hz, OCH_2CH_2), 1.51-1.45 (m, 2H),1.37 -1.27 (m, 24H), 0.88 (t, J = 4 Hz, 3H, CH_2CH_3). HRMS (Q-TOF) calculated for $C_{37}H_{48}NO^+$ ($M+H^+$) m/z 522,3730 found m/z 522,3729.

2.4 Device fabrication.

The bottom-gate, bottom-contact Organic Field-Effect Transistor (OFET) devices were used as provided by Ossila (Sheffield, UK). These OFETs were prepared on heavily doped silicon wafers with a gate insulator consisting of a thermally grown SiO_2 layer (300 nm). Additionally, the source and drain contacts were formed through the thermal evaporation of gold (Au) material. Later on, the semi-conducting layer n-OPIA (4 mg/mL in chlorobenzene) was cast using the solvent vapor enhanced drop casting method at various temperatures (22 °C, 30 °C and 34 °C) and dried overnight. Prior to deposition, these devices were washed with Decon^{TM} solution, water, acetone, and isopropanol for 5 minutes each. Subsequently, the substrates were treated with UV-Ozone cleaning for a period of 20 minutes. 50 µL of self-assembled monolayer (SAM) octadecyltrichlorosilane (OTS-18) in 20 mL of hexadecane was used to functionalize the dielectric layer (SiO_2) for 30 minutes and then washed in chloroform for 5 minutes in order to eliminate the effect of the high contact resistance created by tightly aligned material contact and molecular orbital levels, as in the case of gold and pentacene to increase hole mobility of our n-OPIA products.[20]The field-effect hole mobility was determined using the equation (1),[21] which involves the source-drain current (I_{SD}) in the saturation regime of

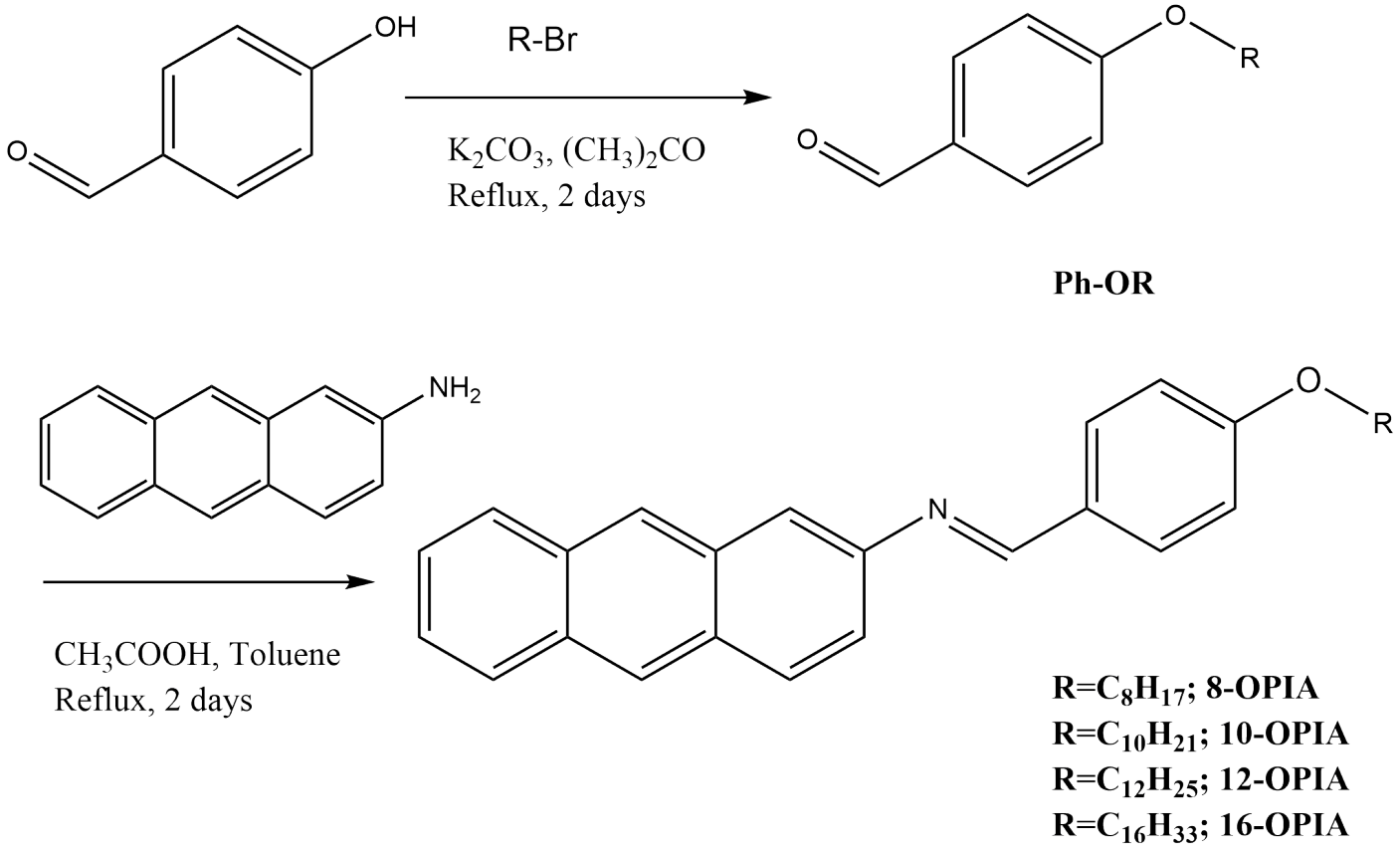

Fig. 1 Synthetic routes of n-OPIA compounds

the transfer characteristics of our OFET devices:

$$I_{SD} = \frac{\mu C_i W (V_{GS} - V_{th})^2}{2L} \quad (1)$$

where μ is the field-effect mobility, L and W are the length and width of the transport channel, C_i is the capacitance per unit area of SiO_2 (C_i= 11.11 nF/cm²), V_{GS} and V_{th} are the transistor gate and threshold voltages, respectively.

3 Results and discussion

3.1 Synthesis and structural characterization.

2-Substituted anthracene derivatives, the (E)-N-(anthracen-2-yl)-1-(4-(alkyloxy) phenyl) methanimine with n = 8, 10, 12, and 16, were designed by combining an alkylated para-hydroxybenzaldehyde moiety and a 2-aminoanthracene moiety. Although para-hydroxybenzaldehyde was chosen to expand the π-conjugation of the core and the alkyloxy chain to introduce mesogenic properties to the compounds. The n-OPIA compounds were synthesized in two steps in good to high yields (Fig. 1). First, the alkylation of para-hydroxybenzaldehyde with several alkyl bromides (octylbromide, decylbromide, dodecylbromide, and hexadecylbromide) by bimolecular nucleophilic substitution. Then an imine coupling of the alkylated para-benzaldehyde with 2-aminoanthracene by nucleophilic addition, as already reported in our earlier work.[18]

3.2 DFT calculation, electrochemical and optical absorption.

UV-vis and cyclic voltammetry (CV) measurements were used to determine the experimental electronic properties of the n-OPIA series and compare them to those obtained from DFT calculations at the B3LYP/6-31G++(d,p) level of theory.

Concerning UV-vis results (Table 1, Figs. 2, S7 and S8), the n-OPIA series in solution showed the same onset absorption at 436, 431, 432, and 431 nm, respectively, for 8-OPIA, 10-OPIA, 12-OPIA, and 16-OPIA, from which their corresponding energy gaps are calculated to be 2.84, 2.87, 2.86, and 2.87 eV. We discover that the absorption peaks of the n-OPIA series exhibited an average red shift of about 19 nm in the thin film compared to the solution form. This shift is due to the greater molecular ordering that gives a good molecular packing geometry in the solid film state.[22,23] Fig. 3 displays an example of CV measurements obtained for 8-OPIA (for CV results of the other homolgous, see Figs. S9 and S10). The exploitation of CV measurements allows the determination of HOMO and LUMO energy levels for n-OPIA homologous.[24] These energy levels are summarized in Table 2. A good agreement was found for HOMO levels from CV and

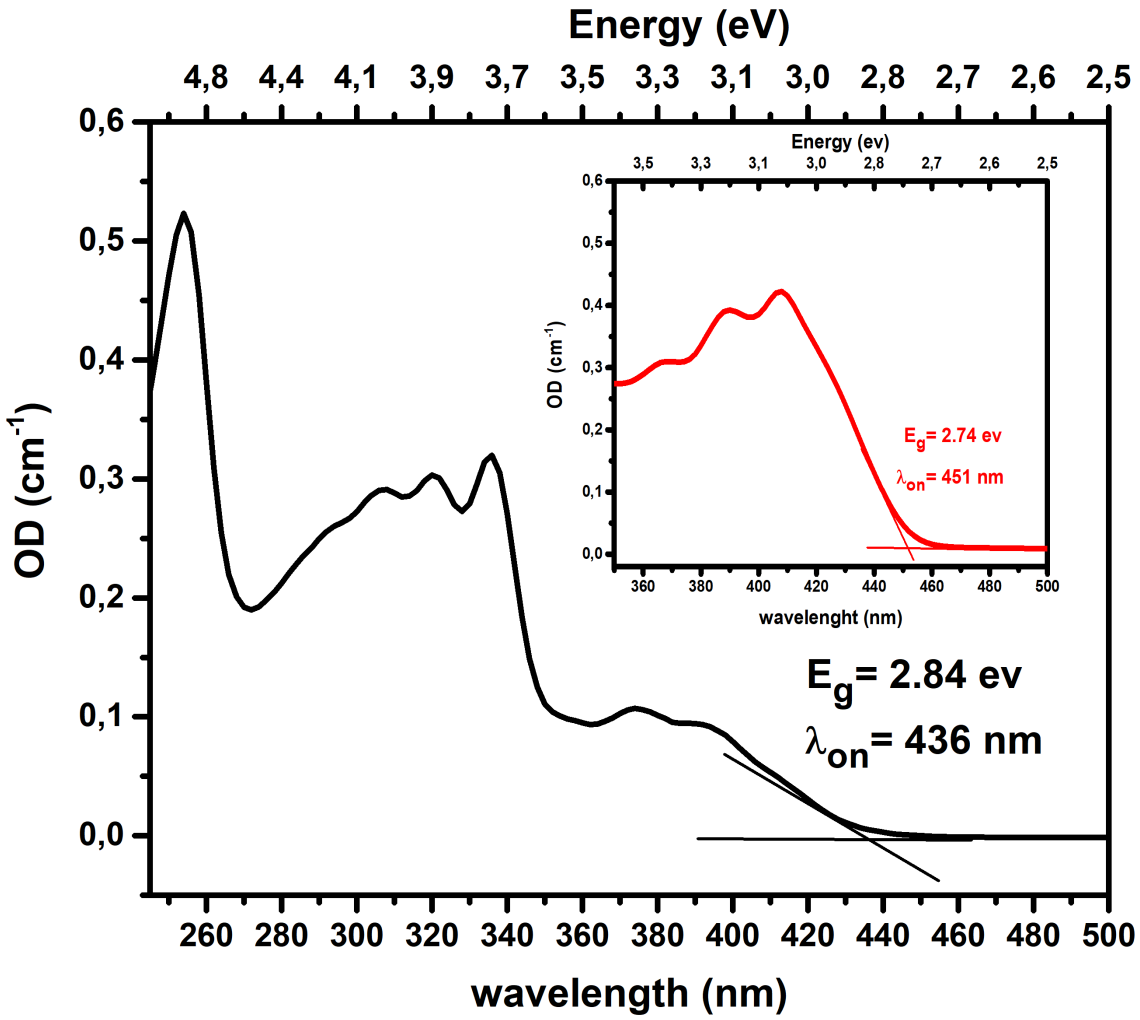

Fig. 2 Example of optical absorption spectrum obtained for 8-OPIA (10^{-5} M solution in dichloromethane). Inset: drop-casted thin film of 8-OPIA (0.5% wt. in chlorobenzene) on a quartz substrate.

DFT for 8-OPIA and 12-OPIA, whereas a small shift was observed for 10-OPIA and 16-OPIA. The measured HOMO values suggest that holes can be easily injected from gold electrodes into n-OPIA films. A difference between LUMO levels determined from CV and DFT was obtained for all n-OPIA compounds: the LUMO values from DFT are smaller than those from CV. As a result, the band gap energies, E_g, from DFT are smaller than those measured by CV method (Table 2), but are in accordance with the values obtained from UV-vis spectroscopy (Table 1).

3.3 Mesomorphic properties.

The mesomorphic properties of n-OPIA compounds were investigated by DSC and POM. Fig. 4 presents the DSC thermograms of the n-OPIA series obtained upon cooling at a rate of 10° C/min, and Fig. 5 shows the microscope capture of textures obtained from POM between crossed polarizers of 16-OPIA. All the n-OPIA compounds display mesomorphic properties between the crystalline (Cr) and isotropic liquid (Iso) phases. The obtained phase transition temperatures were determined by both DSC and POM measurements to explore the effect of alkyloxy chain lengths on the mesomorphic behaviours of the n-OPIA series.

The transition temperatures and the mesophase temperature domains of n-OPIA compounds are gathered in Table 3. 8, 10, and 12-OPIA exhibit three enthalpy peaks, which are assigned to Cr1-Cr2, Cr2-nematic phase (N) and the N-Iso phase transition, whereas for 16-OPIA additional mesophase was observed, namely the lamellar semectic A phase (Sm). For this homologous system, the observed phase transitions are Cr-Sm, Sm-N, and N-Iso. A decrease in melting temperature, MT (from 156 °C to 143 °C), as well as in the temperature stability domain of the mesomorphic behaviour, ΔT_m (from 18 °C to 8 °C), were observed with increasing alkyloxy chain length from 8-OPIA to 16-OPIA.

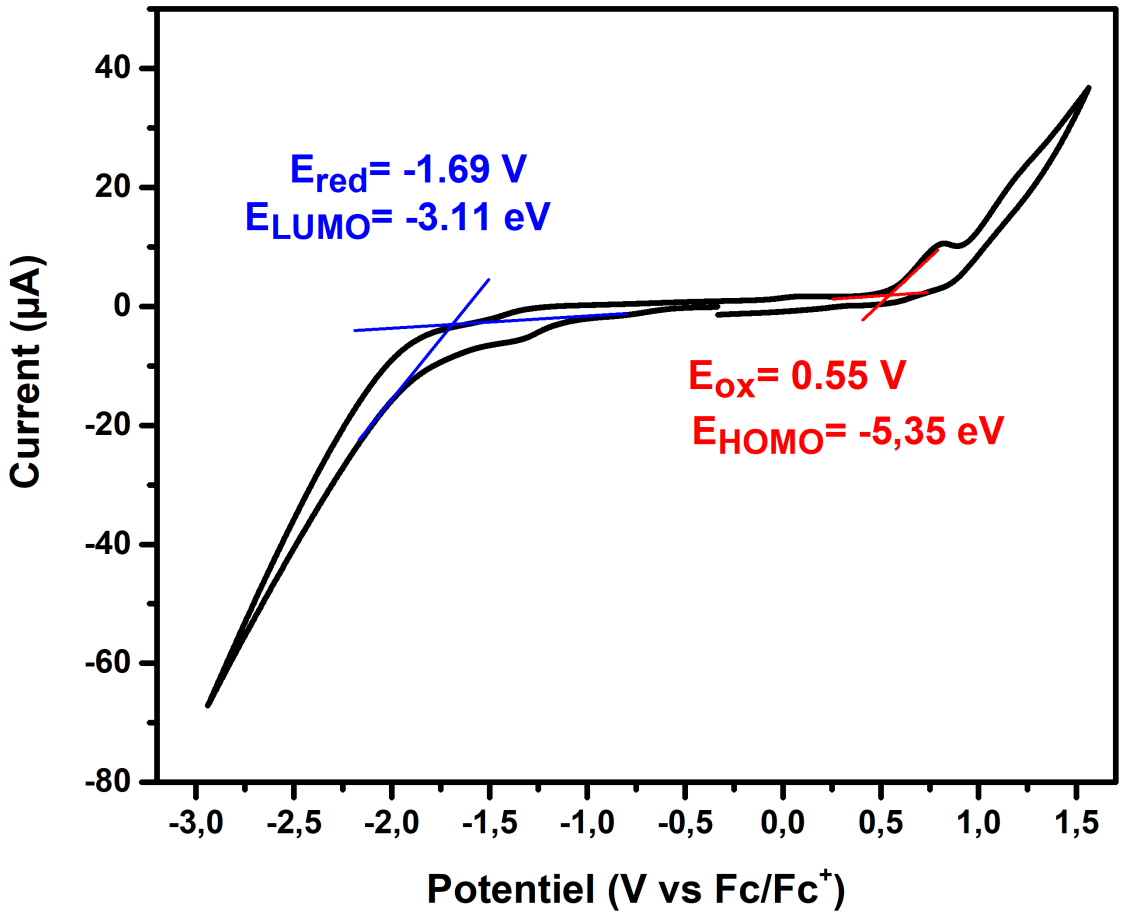

Fig. 3 Cyclic voltammogram obtained for 8-OPIA homologous (2mmol) in 0.1 $TBAPF_6$ in DCM, degassed with Argon (20 minutes) at 50 mV/s versus Fc/Fc+ (Silver wire (RE), platinum disc of 3mm diameter (WE) and platinum wire (CE)).

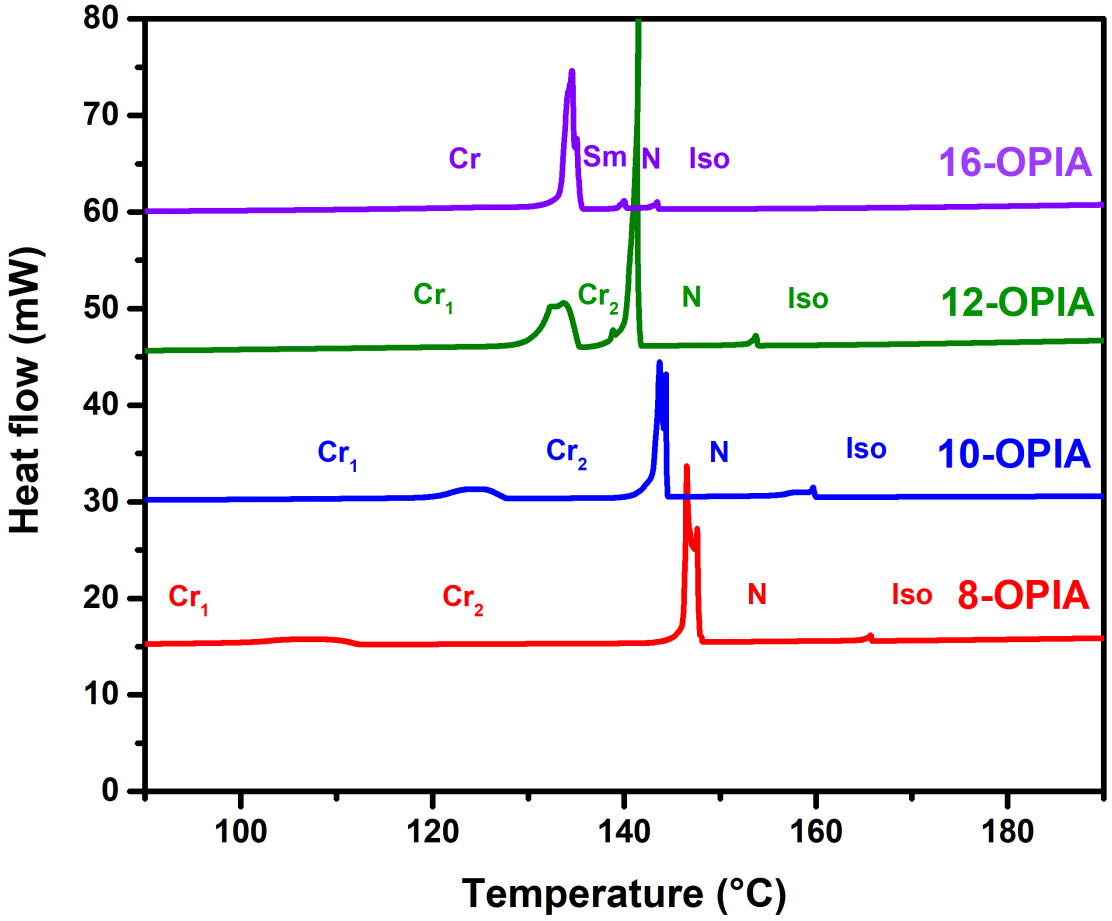

Fig. 4 DSC thermograms of n-OPIA obtained on cooling with a rate of 10°C/min.

Table 1 Optical properties from *UV-Vis* absorption spectra of the n-OPIA series in solution and thin film.

n-OPIA	$\lambda_{UV\text{-}sol}(nm)^a$	$E_{g\text{-}UV\text{-}sol}(eV)^a$	$\lambda_{UV\text{-}film}(nm)^a$	$E_{g\text{-}UV\text{-}film}(eV)^a$
8-OPIA	436	2.84	451	2.74
10-OPIA	431	2.87	453	2.73
12-OPIA	432	2.86	449	2.76
16-OPIA	431	2.87	453	2.73

[a]Note: $\lambda_{UV\text{-}sol}$ Absorption onset wavelength in chloroform solution (10^{-5} M). $\lambda_{UV\text{-}film}$ Absorption onset wavelength of thin films. E_g Optical band gaps calculated from the absorption onset wavelength of solutions and thin films: $E_g = 1236.97/\lambda_{onset}$

Table 2 Electrochemical properties of n-OPIA compounds from DFT calculations and cyclic voltammetry measurements.

n-OPIA	$E_{HOMO\text{-}DFT}$ (eV)	$E_{LUMO\text{-}DFT}$ (eV)	$E_{g\ (HOMO\text{-}LUMO)\ DFT}$ (eV)	$E_{HOMO\text{-}CV}(eV)^a$	$E_{LUMO\text{-}CV}$ (eV)[a]	$E_{g\ (HOMO\text{-}LUMO)\ CV}$ (eV)[a]
8-OPIA	-5.28	-2.03	3.25	-5.35	-3.11	2.25
10-OPIA	-5.27	-2.02	3.25	-5.60	-2.90	2.70
12-OPIA	-5.28	-2.03	3.25	-5.41	-3.03	2.38
16-OPIA	-5,27	-2.02	3.25	-5.68	-3.01	2.67

[a]Note: $E_{HOMO\text{-}CV}$ and $E_{LUMO\text{-}CV}$ calculated from the oxidative potential of CV: $E_{HOMO\text{-}CV} = -(E_{OX} + 4.8)$, $E_{LUMO\text{-}CV} = -(E_{RED} + 4.8)$, and $E_{g\ (HOMO\text{-}LUMO)CV} = E_{HOMO\text{-}CV} - E_{LUMO\text{-}CV}$.

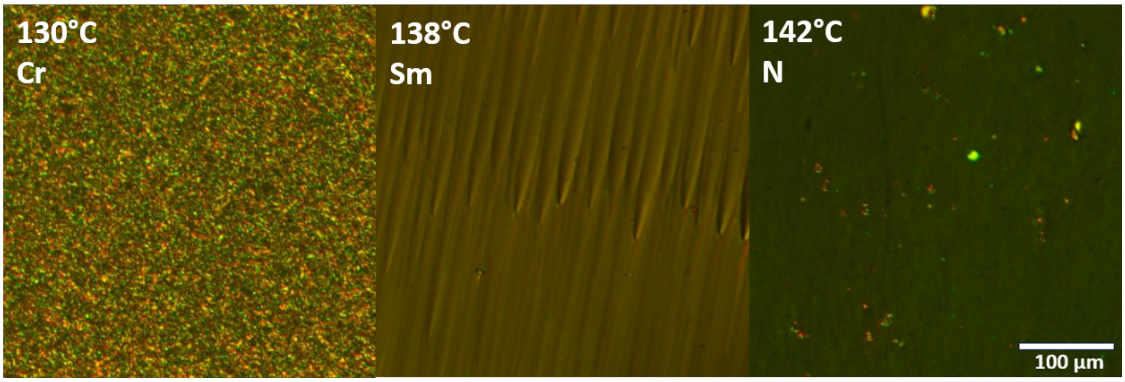

Fig. 5 Microscope capture of textures obtained for 16-OPIA from polarized optical microscope between crossed polarizers upon cooling from isotropic phase to crystalline phase.

Mesophase stability is determined by a balance of two combined effects: the polar effect caused by the interaction of dipole moments in the aromatic part of molecules, which is highly dependent on where the connected polar group is located and promotes a tendency towards order, and the steric effect caused by the length of the lateral alkyloxy chain moiety, which, on the other hand, tends to favour disorder. The decrease in the mesomorphic stability of n-OPIA compounds with increasing alkyloxy chain length can merely be explained by the fact that the steric effect progressively dominates the polar effect as the side chain becomes longer. This mesomorphic behaviour was already observed for non-symmetrical naphthalene based compounds[25] and 2- (and 3-) substituted phenyl 4'-(4''alkyloxy phenylazo) benzoate compounds[26] that show a decrease in mesomorphic stability while increasing the alkyloxy chain length.

3.4 Charge transport properties.

The charge transport properties of the n-OPIA series as p-type were measured using interdigitated (L = 50 µm, W = 18 mm) Ossilla OFET in a bottom-gate (BG), bottom-contact (BC) configuration under ambient conditions at V_{DS} = -100 V. The active semiconducting layer was deposited by the solvent vapour enhanced drop casting method in order to slow down the solvent evaporation and obtain large crystals exceeding the channel length to optimise the hole mobility (Fig. 6). The 8-OPIA and 10-OPIA drop-cast films were deposited at 22 °C, while the 12-OPIA and 16-OPIA films were deposited at 30 °C and 34 °C, respectively, according to their corresponding solubility in chlorobenzene, resulting in film thicknesses around 750 nm. The field-effect mobility, μ, threshold voltage, V_{th}, and on/off current ratio, I_{ON}/I_{OFF} deduced from transfer characteristics at V_{SD} = -100 V, are summarized in Table 4. Fig. 7 a, b, c and d show typical transfer characteristics measured for 8, 10, 12 and 16-OPIA films, respectively. It is significant to note that the electrical field effect parameters of n-OPIA strongly depend on the length of the alkyloxy chain: as the length of the alkyloxy chain increases, the field-effect mobility (Fig. 8) and on/off current ratio decrease by about two orders of magnitude, whereas the threshold voltage slightly decreases. The decrease of field effect mobility in the crystalline phase with the alkyloxy chain length can be attributed to changes in the morphology of drop-casted films. The AFM images displayed in Fig. 9 reveal differences in the surface morphology: the drop-casted 8-OPIA film has fine and continuous grains (Fig. 9 a), while for the deposited 10 and 12-OPIA films (Fig. 9 b and c) have smaller and discontinuous grains with a greater density of grain boundaries (the observed morphology of 16-OPIA is similar to 12-OPIA). As the lateral chain length increases, the film

Table 3 Mesomorphic behaviours of n-OPIA compounds: MT, melting temperature, $T_{Iso\text{-}N}$, phase transition temperature from Iso to N, $T_{N\text{-}Sm}$ phase transition temperature from N to Sm, (ΔT_N) nematic temperature range, and (ΔT_m) mesophase temperature range of n-OPIA compounds.

n-OPIA	MT(°C)	$T_{Iso\text{-}N}$(°C)	$T_{N\text{-}Sm}$ (°C)	ΔT_{N}(°C)	ΔT_{m}(°C)
8-OPIA	156	166	–	18	18
10-OPIA	155	160	–	15	15
12-OPIA	147	154	–	12	12
16-OPIA	143	144	140	4	8

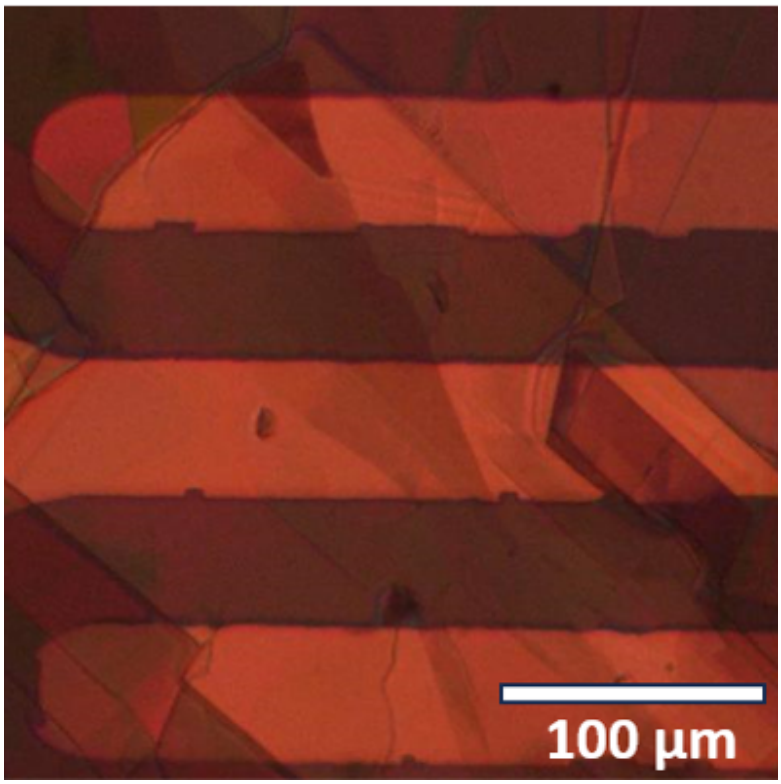

Fig. 6 Microscope capture of texture from 8-OPIA drop-casted OFET film.

morphology changes from continuous to discontinuous crystalline grains, leading to more trapping of charge carriers trapped within the layers, which reduces the hole field-effect mobility.

Similar behaviours on electrical field effect parameters were already observed on non-mesogenic anthracene materials.[27,28] In fact, J.Y. Back et al.[27] have reported measurements of hole mobility on asymmetric alkylated phenyl-anthracene-based molecules with different alkyl side chain lengths. They found that field-effect mobility, threshold voltage, and on/off current ratio depend on alkyl chain length: a decrease in the field-effect hole mobility, in the on/off current ratio of about 2 orders of magnitude, and in the threshold voltage of about 1 order of magnitude, were observed when the number of carbons in the alkyl chain was increased from 5 to 10.

This trend was also observed by Zhang et al.[28] for non-mesomorphic materials with symmetric alkylated diphenyl-anthracene based molecules, where the field-effect hole mobility shows a less drastic decrease with the increases of alkyl side chain length, typically from 3.40 to 0.82 cm^2/V s when the number n of carbon of alkyl chain vary from n = 0 to 6. The authors explained this effect by using more ordered molecular packing structures in the solid film state upon solution processing, when the alkyl chain becomes shorter due to the better solubility with decreasing the length of the alkyl chain. In addition, the same trend was also observed in the case of macromolecular materials.

Y. D. Park et al.[29] reported the effect of alkyl side chain length on the electric properties of regioregular poly(3- alkylthiophene) (P3AT). These authors found that the field-effect mobilities measured on OFET devices for P3AT films based on three side chain lengths (butyl(P3BT), hexyl (P3HT), and octyl (P3OT)) are $1.1.10^{-2}$ cm^2/V s for P3BT with a shorter alkyl chain, which is 20 times greater than 5.2×10^{-4} cm^2/V s measured for P3OT with a longer alkyl side chain. The increase in the field-effect mobilities with increasing the length of the alkyl side chain was explained by the higher density of π-stacked ordered structures of films formed from macromolecules with shorter side chains.[29] A hole mobility value of $(3.2 \pm 1.0) \times 10^{-4}$ cm^2/V s achieved for 8-OPIA is near to that value of 3.9×10^{-4} cm^2/V s reported for anthracene-based arylacetylenes (9,10- bis-[m, p-bis(hexyloxy)phenyl]ethynyl-anthracene)[30]. It is important to know that our OFET measurements are in the BG/BC configuration, which generally gives smaller values of mobilities than those measured in the

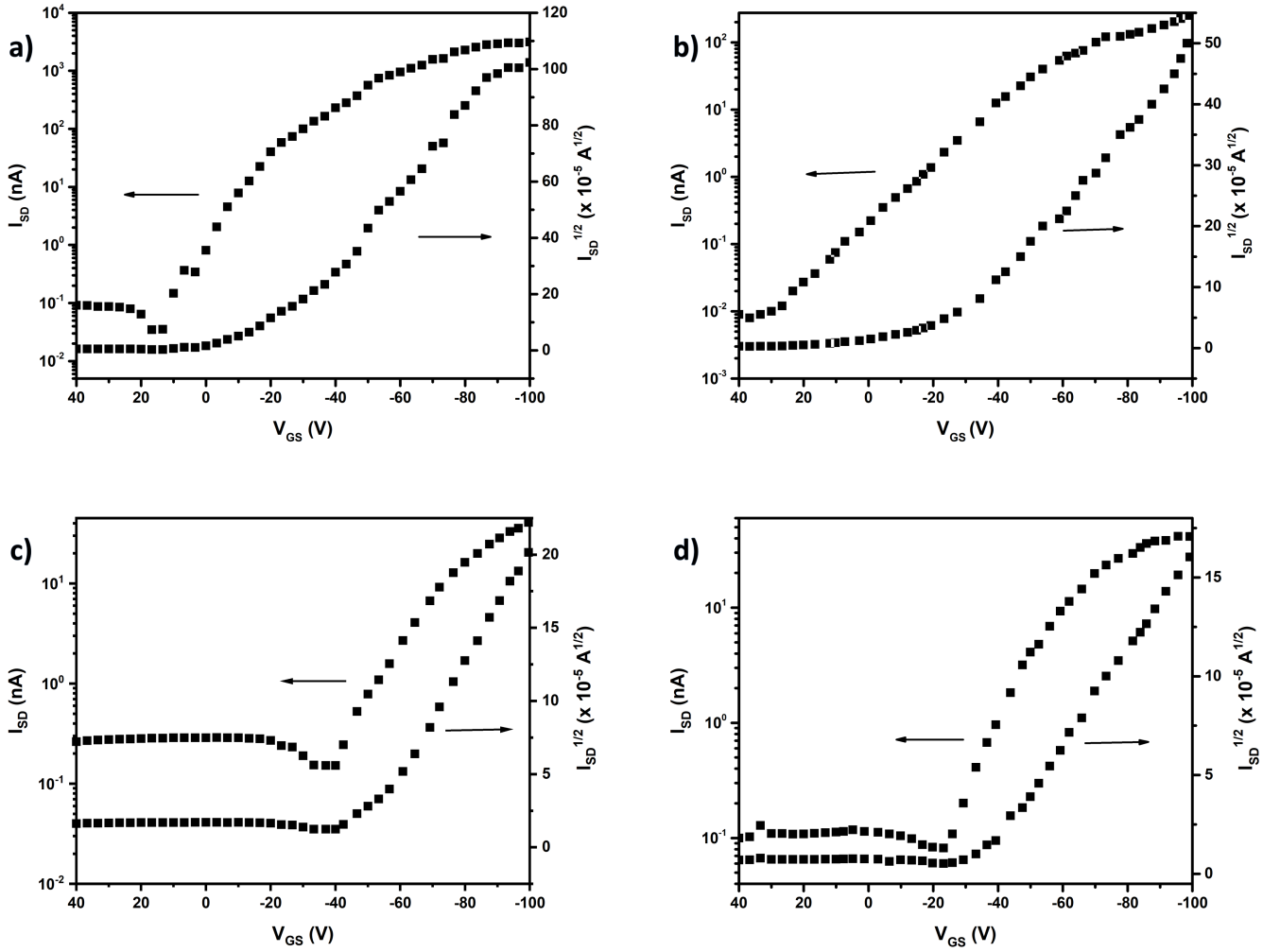

Fig. 7 Transfer characteristics of BG/BC OFETs based drop-casted films: (a) 8-OPIA, (b) 10-OPIA, (c) 12-OPIA and (d) 16-OPIA films.

BG/top contact (TC) configuration.[20]

It is also important to consider how the connection between anthracene and phenyl groups affects hole mobility in anthracene-phenyl-based compounds. Qiu et al.[31] reported asymmetric phenyl anthracene derivatives that differ by the connection bond between anthracene and phenyl, the 2-phenyl-anthracene (2-phA) with a single bond and 2-(phenylvinyl) anthracene (2-phvA) with a double bond. The field effect hole mobility shows a decrease from 0.89 cm^2/V s for 2-PhvA to 1.43 $\times$ 10^{-3} cm^2/V s for 2-PhA that refers to the nature of the connection bond. Based on the AFM and XRD results, the 2-PhvA film morphology was demonstrated to be uniform and smooth, with a well-organized molecular structure, displaying better electrical performance than the discontinous film morphology obtained for 2-PhA, which leads to poor charge transport in OFETs. Consquently, the resulting film morphology and well-organized molecular structure can be related to the torsional capacity of the bond between the phenyl and anthracene groups. Double bonds inhibit rotation while single bonds favour it, promoting a planar structure and stronger π-π interactions for double bonds than single bonds that enhance charge transport properties. Our molecules feature imine bonds between phenyl and anthracene, which act as double bonds by enhancing the mobility of the field effect.

Annealing does not always result in improved mobility, as in our case, annealing the n-OPIA films deposited on OFETs does not improve mobility, but it does reduce it, and this was verified by our studies of Current-Voltage measurements as a function of temperature and revealed by POM observation of film textures, which shows cracks in the deposit films. There was a decrement in the hole mobility from 0.92 cm^2/V s at sublimation temperature of 25 °C to 0.19 cm^2/V s after annealing at 130°C for 5 minutes for 2-(4-octylphenyl)-anthracene.[32]

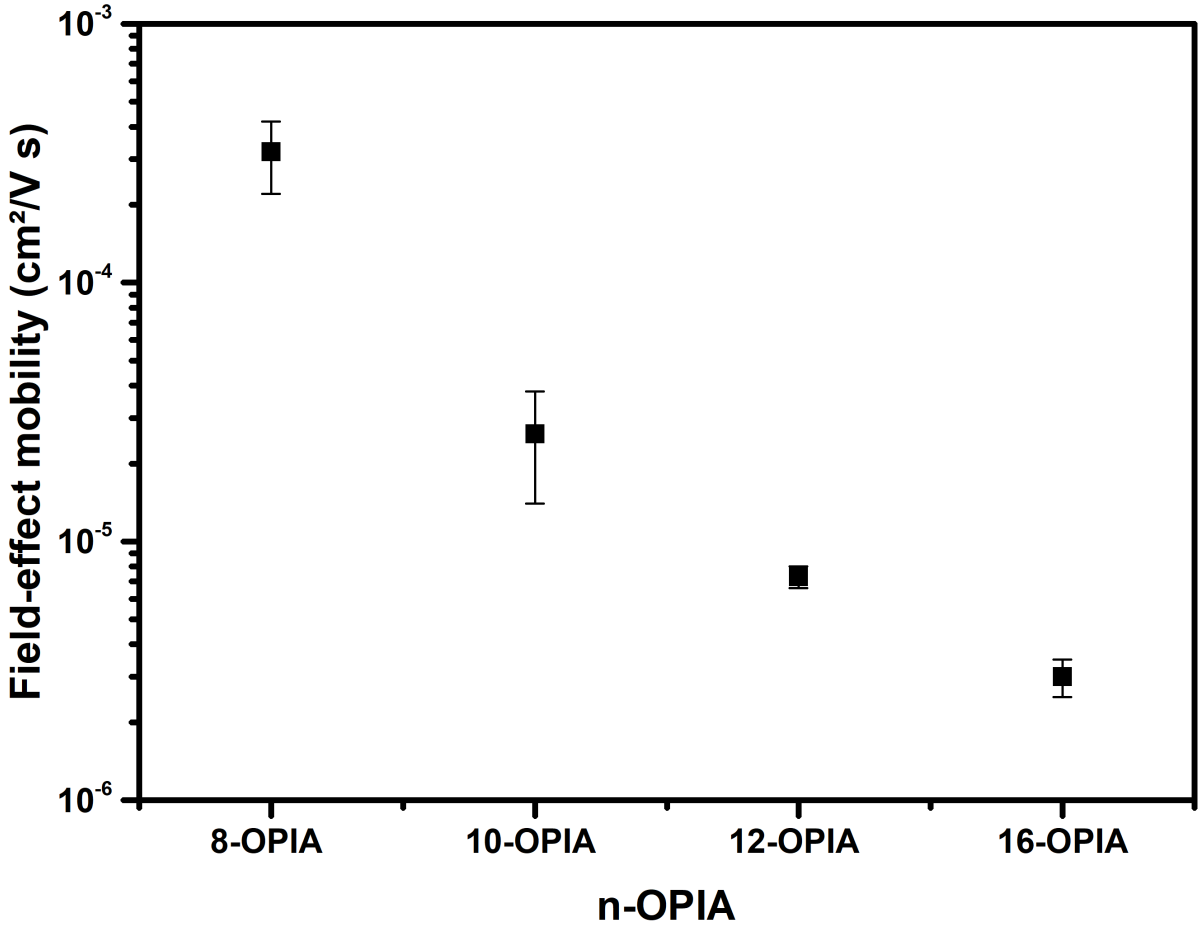

Fig. 8 Dependence of the field-effect mobility on the alkyloxy chain length for n-OPIA compounds.

Table 4 The field-effect mobility, μ, threshold voltage V_{th}, and on/off current ratio, I_{ON}/I_{OFF} of the n-OPIA OFET Devices

n-OPIA	μ (cm^2/Vs)	I_{ON}/I_{OFF}	V_{th} (V)
8-OPIA	(3.2 ± 1.0) x 10^{-4}	8.7 x 10^4	-18
10-OPIA	(2.6 ± 1.2) x 10^{-5}	2.8 x 10^4	-20
12-OPIA	(7.3 ± 0.7) x 10^{-6}	2.9 x 10^2	-40
16-OPIA	(3.0 ± 0.5) x 10^{-6}	5.0 x 10^2	-30

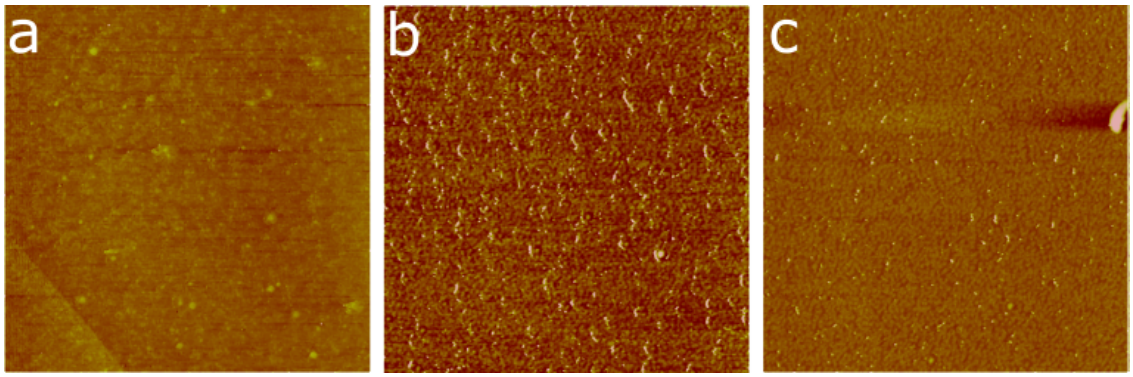

Fig. 9 AFM images (2 µm x 2 µm) of 8 (a), 10 (b) and 12-OPIA (c) drop-casted films on OTS-treated SiO_2 substrate.

3.5 Photoconductive properties.

The transfer characteristics of 8, 10, 12 and 16-OPIA devices obtained under UV-irradiation of λ= 455 nm at an intensity of 2.40 mW/cm² and a source-drain voltage of -100 V were compared with those obtained in the dark condition (Fig. 10 a, b, c and d). The OFET-based n-OPIA films displayed a significant increase in I_{SD} current of about one order of magnitude. When light with a photon energy equal to or greater than the molecular band-gap energy of an organic semiconductor is absorbed, a number of charge carriers are produced, increasing the $_{SD}$ current. This suggests that, in addition to V_{GS}, light may also be used as an additional terminal to optically control the current of OFET device operation.[33,34]

The transfer characteristics of 8-OPIA OFET displayed in Fig. 11 show a gradual increase of I_{SD} as the power density of UV-irradiation increases. Fig. 12 also presents the transfer characteristics of an OFET based drop-casted 8-OPIA film in the dark and under UV-light illumination, which clearly shows a threshold voltage shift. The same behaviour was also observed for all homologous members of the studied n-OPIA series. This effect, well-known as photovoltaic effect, is caused by the accumulation of charge carriers in inorganic and organic phototransistors[35] can explain the threshold voltage shift from V_{Th} to photoinduced one, $V_{Th,Ph}$ and the increase in I_{SD} current.[36–38] Another effect that can explain the threshold voltage shift is the bias stress effect, which is caused by electrons trapped in organic semiconductors.[39–41]

Under illumination, the measured $V_{Th,Ph}$ for the n-OPIA devices reached 55 V, 20 V, 40 V, and 30 V for 8-OPIA, 10-OPIA, 12-OPIA, and 16-OPIA, respectively. A threshold voltage shift under illumination to a value of about 30 V was also obtained for the 2,5-bis-biphenyl-4-yl-thieno[3,2-b]thiophene (BPTT) and pentacene.[36]

The photosensitivity of 8-OPIA OFET, defined as the I_{Ph}/I_{Dark} ratio, was determined as a function of incident power and presented in Fig. 13. This photosensitivity was evaluated at switch on voltage V_{GS} = -22 V to eliminate the impact of hole carriers induced by the gate electrode. A maximum photosensitivity of 3.0 x 10^5 is reached under a power UV-light irradiation of about 50 µW. This exceptional photosensitivity is the double of that found for pentacene as a p-type organic semiconductor phototransistor (1.3 x 10^5).[36]

The responsivity, R (defined as I_{Ph} over the incident optical power) was also examined for n-OPIA OFETs to determine the influence of alkyloxy chain length on their photoresponse. As observed from Fig. 14, R continuously decreases by around two orders of magnitude as the alkyloxy chain length increases. The low responsivity of our homologous n-OPIA film can be attributed to the internal filter effect[42] of n-OPIA films, which act as filters, absorbing light irradiation with wavelengths in their absorption spectrum. This allows a low intensity of irradiation to pass through the film to the interface between the semiconductor and the dielectric layers (the first molecular layers adjacent to the dielectrics form an effective charge flow layer for charge transport in OFETs[43]). That emphasize how crucial it is to select a wave length which can reach the semiconductor-dielectric interface without being absorbed by the semiconductor.

Noh et al.[42] found that changing the irradiation wavelength improved the responsitivity of OPET-based Pentacene. An increase in responsivity from 0.45 A/W to 45 A/W when changing the wavelength from 650 nm to 365 nm was attributed to this internal filter effect. Another parameter that can influence R is the channel length L. In fact, it was already reported[44] that R decreases by three order of magnitudes as L increases from 2.5 µm to 20 µm for N,N'-alkyl perylenebis(dicarboximide) (PDI-C_n) thin film organic phototransistors (tf-OPT). In our studies, we used OFET with a channel length of 50 µm, which resulted in low responsivity. We are currently studying the relationship between R and L for our OFETs based n-OPIA films (work in progress).

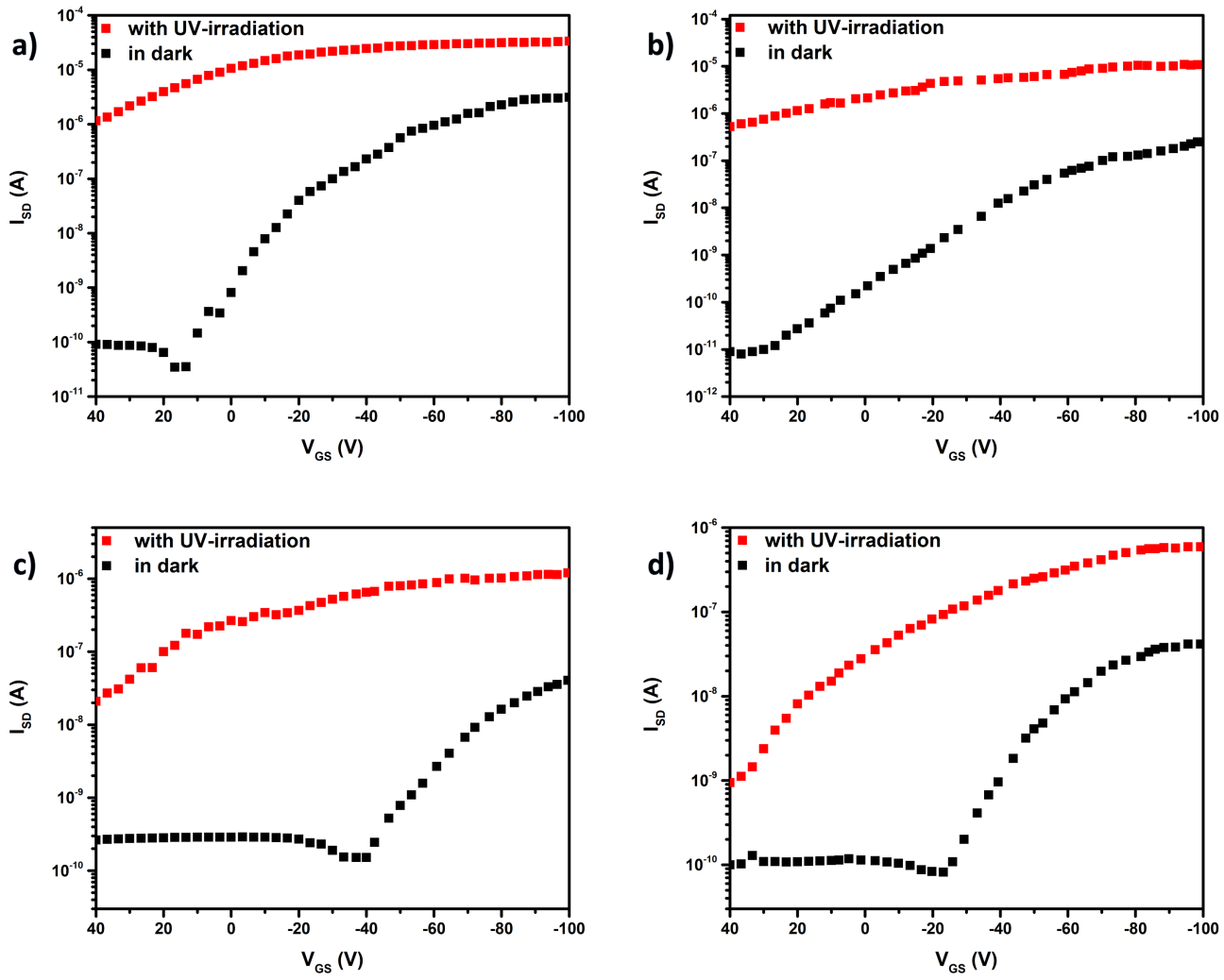

Fig. 10 Transfer characteristics of OFETs based drop-casted films: a) 8-OPIA, b) 10-OPIA, c) 12-OPIA and d) 16-OPIA films in the dark and under UV-irradiation (λ= 455 nm at a power of 21.6 µW) at V_{SD}= -100 V.

4 Conclusions

The new homologous series of asymmetric anthracene derivatives has been synthesised and characterised to study the effect of alkyloxy chain length on the performance of OFET in the dark and under UV-irradiation. These derivatives exhibit liquid-crystalline and semiconducting characteristics based on their molecular structure, which consists of an anthracene core conjugated to a phenyl for conduction and to an alkyloxy chain to generate mesomorphic behaviour. This series was well characterised chemically by NMR and MS and for their mesomorphic behaviours by DSC and POM. A decrease in melting point and mesophase temperature range with alkyloxy chain length. Their electrochemical properties were characterized by UV-vis and CV and compared with DFT calculations that mention a shallow barrier for hole injection from the Au electrode and stability under ambient conditions.

Multifunctional applications of drop-casted n-OPIA films as p-type were characterised by OFET devices in the dark and under illumination, which caused a decrease in the hole mobility, on/off current ratio, and responsivity of n-OPIA compounds with increasing alkyloxy chain length. The best obtained mobility ($(3.2 \pm 1.0) \times 10^{-4}$ cm²/V s) and responsivity (0.2 A/W) are for the 8-OPIA homologous. These results underline the importance of our newly synthesised liquid crystal series as a semiconductor for constructing solution processable hole-transporting materials for organic electronics, in particular optoelectronic devices like phototransistors and photodetectors.

5 Conflicts of interest

There are no conflicts to declare.

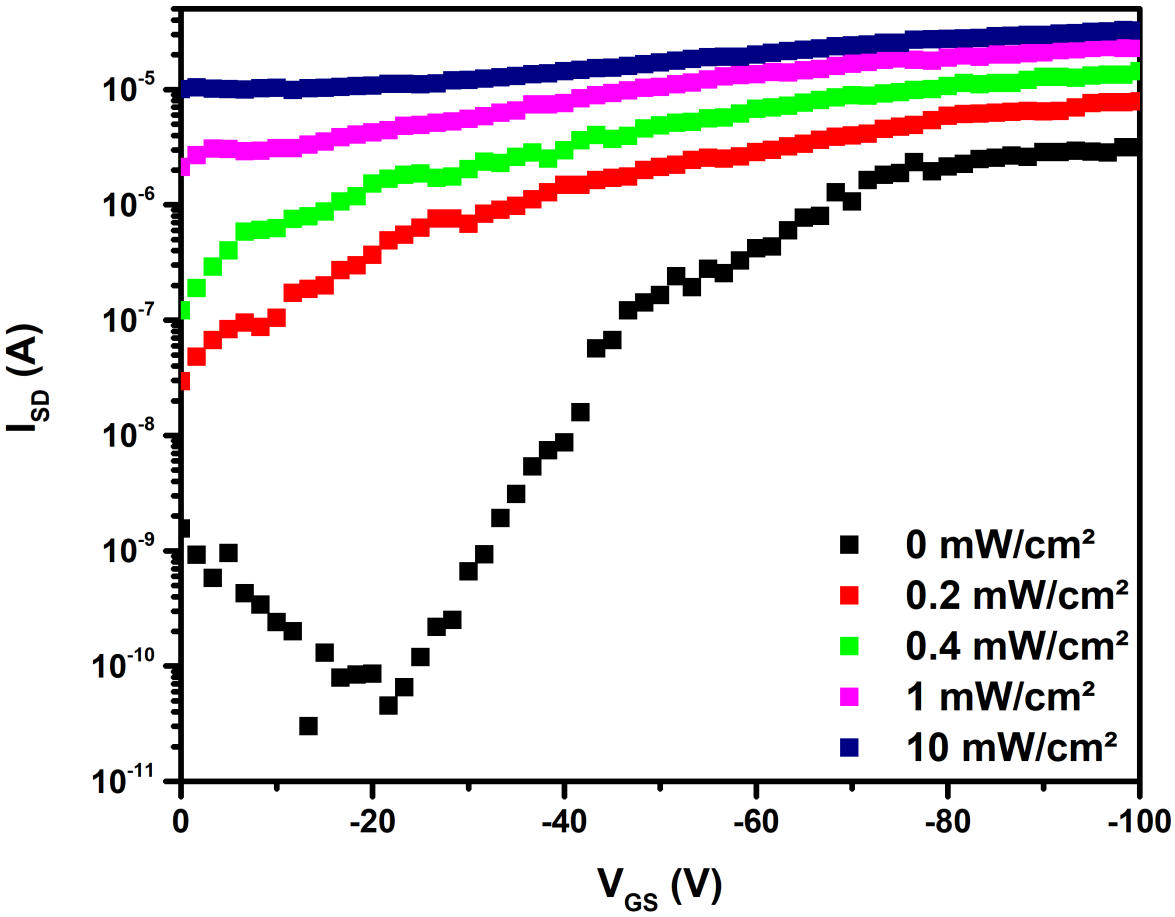

Fig. 11 Transfer characteristics of an OFET based drop-casted 8-OPIA film as a function of UV-light intensity at λ = 455 nm (V_{SD} = - 100 V).

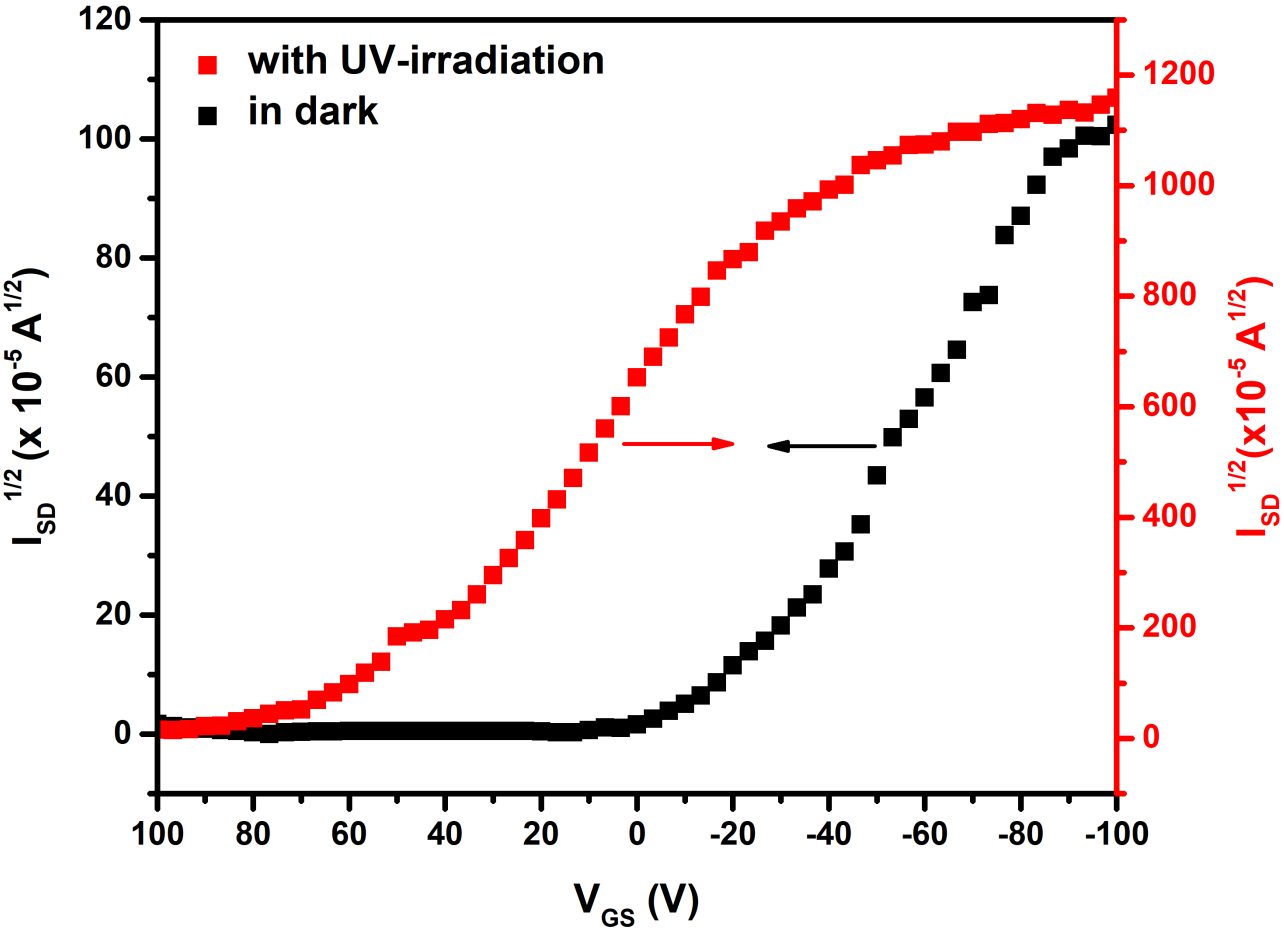

Fig. 12 Transfer characteristics of an OFET based drop-casted 8-OPIA film in the dark and under UV-light illumination (λ= 455 nm at a power of 21.6 μW) showing the threshold voltage shift.

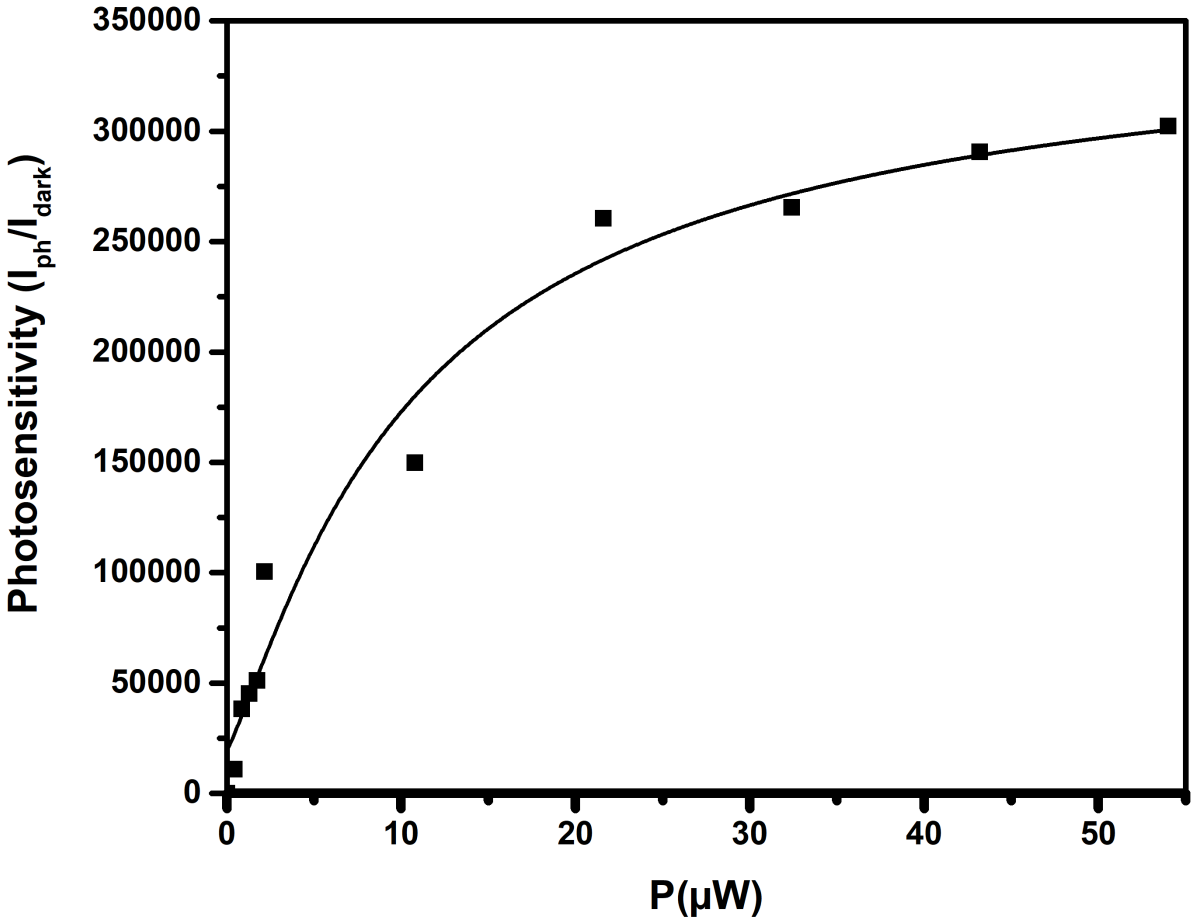

Fig. 13 Photosensitivity (I_{ph}/I_{dark}) as a function of incident UV-light power of OFET based drop-casted 8-OPIA film (V_{GS}= -22 V).

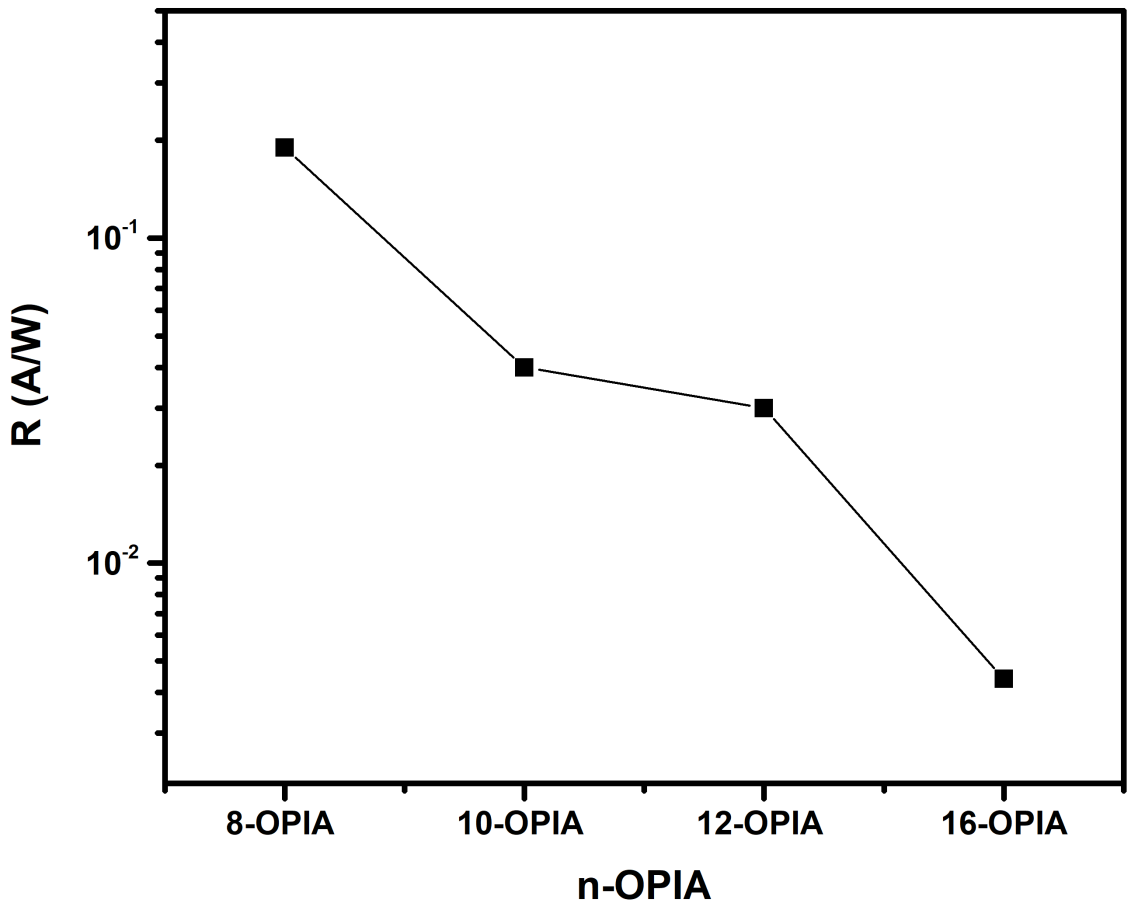

Fig. 14 The responsivity of n-OPIA OFETs as a function of alkyloxy chain length under illumination (P= 21.6 μW) at V_{GS}= −22 V and V_{SD}= −100 V.

6 Acknowledgements

The authors appreciate funding support from ULCO and Region Hauts-de-France. MA is grateful to Mohammed EL AMINE ZAIR for the DFT calculations and Benoit DUPONCHEL for the AFM measurements.

References

1 Q. Tang, Y. Tong, W. Hu, Q. Wan and T. Bjørnholm, *Adv. Mater.*, 2009, 21, 4234–4237.
2 S. R. Forrest, *nature*, 2004, 428, 911–918.
3 H.-R. Tseng, H. Phan, C. Luo, M. Wang, L. A. Perez, S. N. Patel, L. Ying, E. J. Kramer, T.-Q. Nguyen, G. C. Bazan *et al.*, *Adv. Mater*, 2014, 26, 2993–2998.
4 H. Yan, Z. Chen, Y. Zheng, C. Newman, J. R. Quinn, F. Dötz, M. Kastler and A. Facchetti, *Nature*, 2009, 457, 679–686.
5 J. E. Anthony, *Chem. Rev.*, 2006, 106, 5028–5048.
6 Q. Ye and C. Chi, *Chem. Mater.*, 2014, 26, 4046–4056.
7 H. Meng, F. Sun, M. B. Goldfinger, G. D. Jaycox, Z. Li, W. J. Marshall and G. S. Blackman, *J. Am. Chem. Soc.*, 2005, 127, 2406–2407.
8 J. Li, K. Zhou, J. Liu, Y. Zhen, L. Liu, J. Zhang, H. Dong, X. Zhang, L. Jiang and W. Hu, *J. Am. Chem. Soc.*, 2017, 139, 17261–17264.
9 J. Liu, H. Zhang, H. Dong, L. Meng, L. Jiang, L. Jiang, Y. Wang, J. Yu, Y. Sun, W. Hu *et al.*, *Nat. Commun.*, 2015, 6, 10032.
10 K. Ito, T. Suzuki, Y. Sakamoto, D. Kubota, Y. Inoue, F. Sato and S. Tokito, *Angew. Chem. Int. Ed.*, 2003, 42, 1159–1162.
11 M. Chen, L. Yan, Y. Zhao, I. Murtaza, H. Meng and W. Huang, *J. Mater. Chem. C.*, 2018, 6, 7416–7444.
12 D. S. Chung, J. W. Park, J.-H. Park, D. Moon, G. H. Kim, H.-S. Lee, D. H. Lee, H.-K. Shim, S.-K. Kwon and C. E. Park, *J. Mater. Chem.*, 2010, 20, 524–530.
13 H. Iino, T. Usui and J.-i. Hanna, *Nat. Commun.*, 2015, 6, 6828.
14 Y. He, M. Sezen, D. Zhang, A. Li, L. Yan, H. Yu, C. He, O. Goto, Y.-L. Loo and H. Meng, *Adv. Electron. Mater.*, 2016, 2, 1600179.
15 Y. He, W. Xu, I. Murtaza, D. Zhang, C. He, Y. Zhu and H. Meng, *RSC Adv.*, 2016, 6, 95149–95155.
16 S. Méry, D. Haristoy, J.-F. Nicoud, D. Guillon, H. Monobe and Y. Shimizu, *J. Mater. Chem.*, 2003, 13, 1622–1630.
17 T. Kato, M. Yoshio, T. Ichikawa, B. Soberats, H. Ohno and M. Funahashi, *Nat. Rev. Mater.*, 2017, 2, 1–20.
18 K. Kondratenko, I. Carlescu, P.-E. Danjou, Y. Boussoualem, A. Simion, B. Duponchel, J.-F. Blach, C. Legrand, N. Hurduc and A. Daoudi, *Phys. Chem. Chem. Phys.*, 2021, 23, 13885–13894.
19 F. A. Cotton, G. Wilkinson, C. A. Murillio and M. Bochmann, *Advanced Inorganic Chemistry*, Wiley, Chichester, 6th edn, 1999.
20 C. Liu, Y. Xu and Y.-Y. Noh, *Mater. Today*, 2015, 18, 79–96.
21 H. Li, N. Tessler and J.-L. Brédas, *Adv. Funct. Mater.*, 2018, 28, 1803096.
22 F. C. Spano, *Annu. Rev. Phys. Chem.*, 2006, 57, 217–243.
23 J.-H. Park, D. H. Lee, H. Kong, M.-J. Park, I. H. Jung, C. A. Park and H.-K. Shim, *Org. Electron.*, 2010, 11, 820–830.
24 M. L. Tang, A. D. Reichardt, P. Wei and Z. Bao, *J. Am. Chem. Soc.*, 2009, 131, 5264–5273.
25 H. A. Ahmed and M. A. El-Atawy, *Liq. Cryst.*, 2021, 48, 1940–1952.
26 M. M. Naoum, N. H. Metwally, M. M. Abd Eltawab and H. A. Ahmed, *Liq. Cryst.*, 2015, 42, 1351–1369.
27 J. Y. Back, T. K. An, Y. R. Cheon, H. Cha, J. Jang, Y. Kim, Y. Baek, D. S. Chung, S.-K. Kwon, C. E. Park *et al.*, *ACS Appl. Mater. Interfaces*, 2015, 7, 351–358.
28 D. Zhang, S. Yokomori, R. Kameyama, C. Zhao, A. Ueda, L. Zhang, R. Kumai, Y. Murakami, H. Meng and H. Mori, *ACS Appl. Mater. Interfaces*, 2020, 13, 989–998.
29 Y. D. Park, D. H. Kim, Y. Jang, J. H. Cho, M. Hwang, H. S. Lee, J. A. Lim and K. Cho, *Org. Electron.*, 2006, 7, 514–520.
30 F. Silvestri, A. Marrocchi, M. Seri, C. Kim, T. J. Marks, A. Facchetti and A. Taticchi, *J. Am. Chem. Soc.*, 2010, 132, 6108–6123.
31 F. Qiu, Y. Dong, J. Liu, Y. Sun, H. Geng, H. Zhang, D. Zhu, X. Shi, J. Liu, J. Zhang *et al.*, *J. Mater. Chem. C*, 2020, 8, 6006–6012.
32 Y. Wang, D. Fang, T. Fu, M. U. Ali, Y. Shi, Y. He, Z. Hu, C. Yan, Z. Mei and H. Meng, *Mater. Chem. Front.*, 2020, 4, 3546–3555.
33 A. J. Seeds and A. De Salles, *IEEE Trans. Microw. Theory Tech.*, 1990, 38, 577–585.
34 A. Madjar, P. R. Herczfeld and A. Paolella, *IEEE Trans. Microw. Theory Tech.*, 1992, 40, 1681–1691.
35 C.-S. Choi, H.-S. Kang, W.-Y. Choi, H.-J. Kim, W.-J. Choi, D.-H. Kim, K.-C. Jang and K.-S. Seo, *IEEE Photon. Technol. Lett.*, 2003, 15, 846–848.
36 Y.-Y. Noh, D.-Y. Kim, Y. Yoshida, K. Yase, B.-J. Jung, E. Lim and H.-K. Shim, *Appl. Phys. Lett.*, 2005, 86, 043501.
37 C.-S. Choi, H.-S. Kang, W.-Y. Choi, H.-J. Kim, W.-J. Choi, D.-H. Kim, K.-C. Jang and K.-S. Seo, *IEEE Photon. Technol. Lett.*, 2003, 15, 846–848.
38 Y. Xu, P. R. Berger, J. N. Wilson and U. H. Bunz, *Appl. Phys. Lett.*, 2004, 85, 4219–4221.
39 D. Knipp, R. Street, A. Völkel and J. Ho, *J. Appl. Phys.*, 2003, 93, 347–355.
40 S. Zilker, C. Detcheverry, E. Cantatore and D. De Leeuw, *Appl. Phys. Lett.*, 2001, 79, 1124–1126.

41 A. Salleo and R. Street, *J. Appl. Phys.*, 2003, 94, 471–479.
42 Y.-Y. Noh, D.-Y. Kim and K. Yase, *J. Appl. Phys.*, 2005, 98, 074505.
43 G. Horowitz, *Adv. Funct. Mater.*, 2003, 13, 53–60.
44 M. El Gemayel, M. Treier, C. Musumeci, C. Li, K. Mullen and P. Samori, *J. Am. Chem. Soc.*, 2012, 134, 2429–2433.